General Fabrication of Monolayer SnO_2 Nanonets for High-Performance Ultraviolet Photodetectors

*Hao Chen, Linfeng Hu, Xiaosheng Fang, and Limin Wu**

A facile approach for the fabrication of monolayer SnO_2 nanonet is presented using polymer colloid monolayer nanofilms from oil–water interface self-assembly as sacrificial templates. The hole size of the nanonets can be adjusted easily by the mean diameter of polymer colloidal spheres. This method can be extended to the fabrication of a series of monolayer nanonets of semiconducting oxides such as TiO_2, ZnO, and CeO_2. Furthermore, the first photoresponse nanodevice based on monolayer SnO_2 nanonet is fabricated. This device presents ultrahigh photocurrent and sensitivity, excellent stability, and reproducibility.

1. Introduction

In recent decades, the fabrication of 2D periodical porous arrays has drawn great interest because such structures often have unusual properties due to scattering of electromagnetic waves on the subwavelength scale.[1–3] As a result, their arrays have applications in nanophotonics, surface-enhanced Raman spectroscopy (SERS), and biosensors.[4–10]

Several interesting strategies for the fabrication of regular porous membranes have been developed. Some of these have involved focused ion-beam milling of preformed thin film, physical deposition, and etching through masks patterned by poly(dimethylsiloxane) (PDMS) stamps, electron-beam lithography, laser interference holography, and chemical deposition by templating against anodic aluminum oxide.[1–3,11–15] However, most of these methods require expensive equipment and long run times.[16] Solution-based self-assembly of colloidal spheres has been demonstrated to be inexpensive, simple, inherently parallel, and high-throughput.[17–22] It has been widely used to fabricate 2D and 3D functional patterns, such as ordered porous films, macroporous materials, and array of rings.[18,19,23] Recently, oil–water planar interfaces have been considered as ideal templates for the self-assembly of various low-dimensional nanostructures into functional monolayers or nanofilms and have received intensive attention.[24–26] Various inorganic and organic colloid nanoparticles, such as Au, Pt, SiO_2, FePt, Ag, $CoPt_3$, Fe_2O_3, polystyrene, and 1D nanostructures; 2D nanoplatelets; and exfoliated nanosheets have been successfully assembled at oil/water interfaces for the fabrication of nanofilms.[18,27–37] Very recently, we have reported the first $NiCo_2O_4$-nanofilm-based photodetector and ZnO hollow-sphere nanofilm-based photodetector based on oil/water interface self-assembly.[38,39] High sensitivity, excellent stability, and fast response time show that 2D structure nanofilms have potential applications in the photodetector field.

Here, we describe the fabrication of a 2D ordered porous SnO_2 monolayer nanofilm (namely, a nanonet) with the monolayer poly(styrene-*co*-acrylic acid) (PSA) colloid crystal nanofilm prepared from oil–water interfacial self-assembly as the template. Unlike previous fabrication procedures, the regular monolayer structure of colloid crystal polymer template used can guarantee homogeneous filtration of SnO_2 precursor into the voids between polymer spheres, thus high quality monolayer SnO_2 nanonets can be fabricated. In addition, the aqueous colloidal polymer particles are directly dispersed into the water phase rather than the oil phase for oil–water interfacial self-assembly.[18] This greatly decreases the cost and time of fabrication. This method can be extended to the fabrication of series of 2D ordered semiconducting nanofilms, such as TiO_2, ZnO, and CeO_2 nanofilms, and some non-semiconductor oxides, such as SiO_2, MgO, and CaO nanofilms. We also constructed the first photoresponsive nanodevice based on monolayer SnO_2 nanonets. Experiments showed that this device has ultrahigh photocurrent and sensitivity, suggesting that this type of ordered porous nanofilm-based nanodevice could be used in high-performance photodetectors, photoelectronic switches, and solar cells.

2. Results and Discussion

2.1. Fabrication of Polymer Monolayer Nanofilm

Scheme 1a–c briefly describes the fabrication of colloid polymer monolayer nanofilm through oil–water interfacial self-assembly. First, 0.05 mL of polymer colloid was dispersed in 40 mL of deionized water to form an aqueous suspension. Then 10 mL of hexane was added to produce a hexane/water interface. When an appropriate amount of ethanol was slowly added by syringe to the interface as an inducer, polymer colloidal spheres immediately migrated to the interface and formed a colloidal

Dr. H. Chen, Dr. L. F. Hu, Prof. X. S. Fang, Prof. L. M. Wu
Department of Materials Science
and Advanced Materials Laboratory
Fudan University
Shanghai 200433, P. R. China
E-mail: lmw@fudan.edu.cn

DOI: 10.1002/adfm.201102506

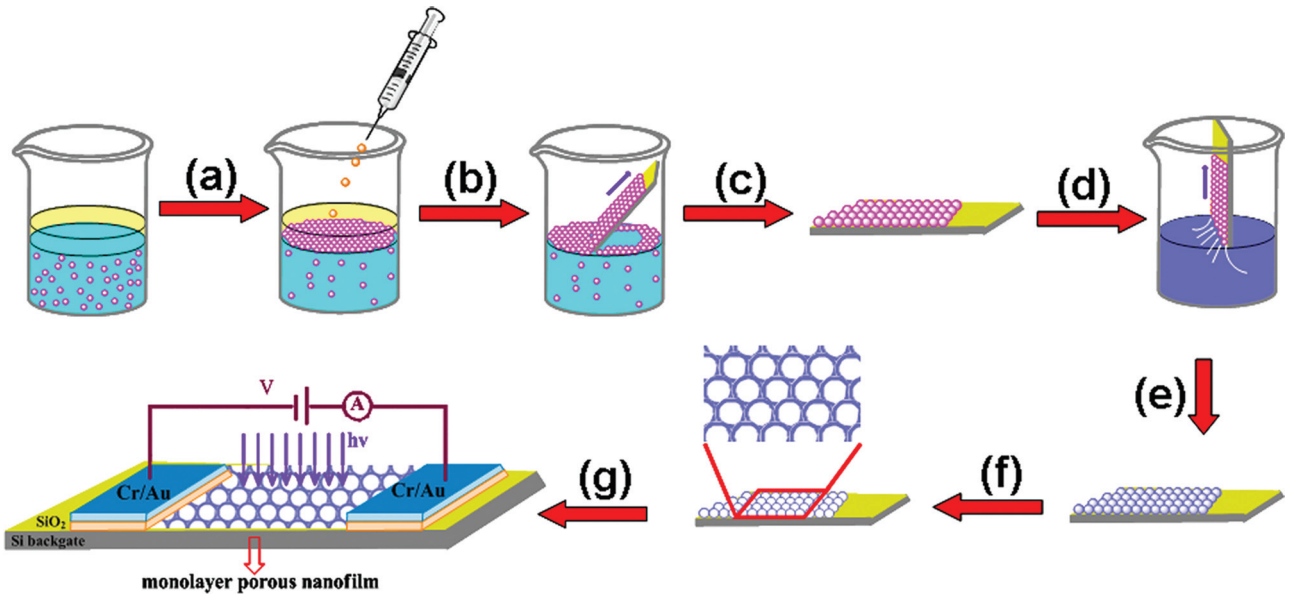

Scheme 1. Schematic illustration of the fabrication of polymer monolayer nanofilm, 2D oxide monolayer nanofilms, and photoresponse nanodevices. a) Addition of ethanol at a hexane/water interface acts as the inducer and the self-assembly of PSA colloids occurrs at the interface. b) Removal of the hexane phase by syringe and transfer of the as-assembled PSA nanofilm on a silicon substrate. c) Drying of PSA colloidal crystal film. d) Filling of the voids in PSA colloidal crystal film with a oxide sol-gel precursor. e) Drying of the infiltrated samples at 40 °C for 10 h. f) Thermal transformation from PSA/oxide film into ordered oxide monolayer nanofilms. g) Schematic illustration of photoresponse nanodevice.

crystal film. The surface pressure from interfacial tension at the hexane/water interface compressed the interfacial colloids into a close-packed structure, which is the key to obtaining ordered monolayer nanofilms.[29] After careful removal of most of the hexane by a syringe, the as-assembled crystal polymer monolayer nanofilm was easily transferred onto a thermally oxidized Si substrate covered with a 200 nm SiO_2 layer.

Figure 1a shows a typical scanning electron microscopy (SEM) image of the monolayer nanofilm from polymer colloids that are 308 nm in diameter. From the cross-sectional SEM image (Figure 1b), the monolayer film thickness can be seen to be equal to the diameter of the polymer microsphere. The as-transformed monolayer polymer film has an area measured in square centimeters, as shown in **Figure 2**. It shows an angle-dependent color, indicating its good 2D long-range order.

2.2. Fabrication of SnO_2 Nanonets

With this monolayer polymer nanofilm as a template, a precursor solution of SnO_2 was allowed to fill the voids between polymer spheres. Then calcination was performed in air at 600 °C. As shown in Scheme 1d–f, 2D ordered SnO_2 monolayer nanofilms were easily fabricated. **Figure 3** shows SEM images of the as-obtained 2D ordered SnO_2 monolayer nanofilms with mean hole size of 251 nm, wall thickness of 67 nm, and thickness of 94 nm. Because the thermal transformation of precursor into oxide leads to shrinkage of the filling volume, the mean hole size and thickness of porous SnO_2 nanofilms are smaller than the mean polymer size of the monolayer film template (≈308 nm). The concentration of precursor solution plays an important role in fabricating high-quality 2D porous SnO_2 monolayer nanofilms. Concentrations below a certain level give thin and

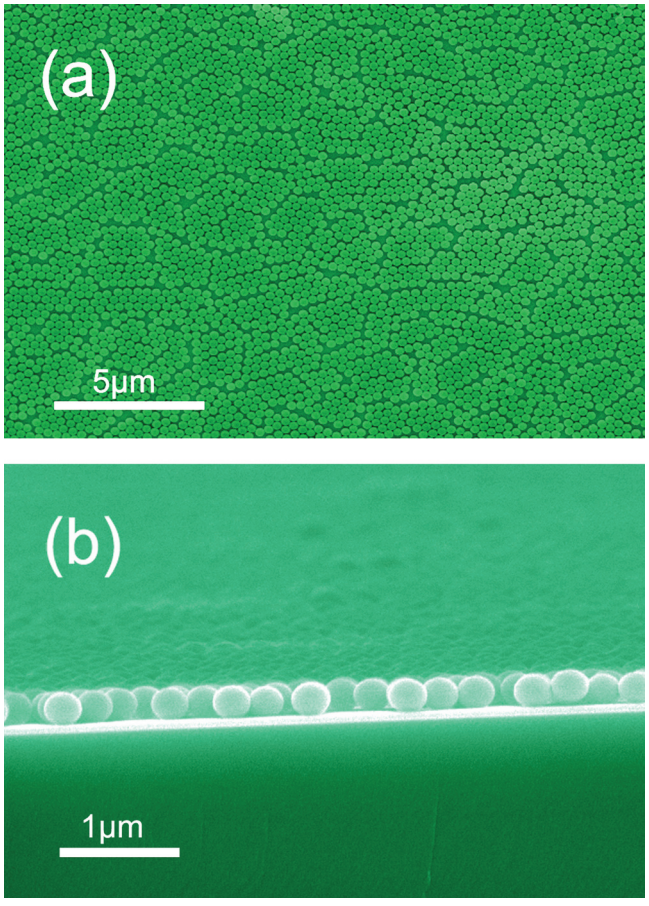

Figure 1. a) Surface SEM image of monolayer polymer film and b) cross-sectional SEM image.

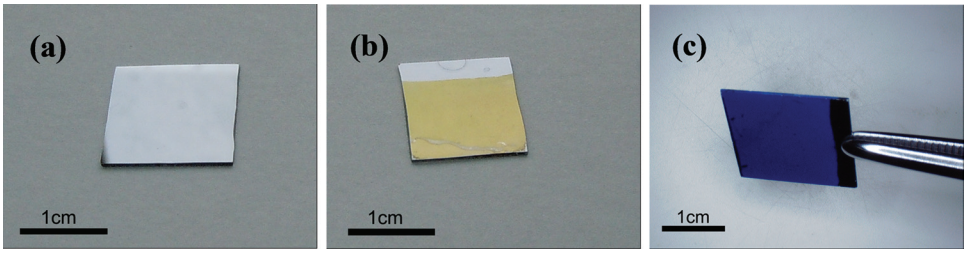

Figure 2. Photographs of silicon wafer and monolayer polymer films: a) silicon wafer under natural light, shooting angle: 45°, b) monolayer polymer film on silicon wafer under natural light, shooting angle: 45°, c) monolayer polymer film on silicon wafer under parallel light, light incident angle: 75°, shooting angle: 75°. All angles were measured based on the surface normal of the sample.

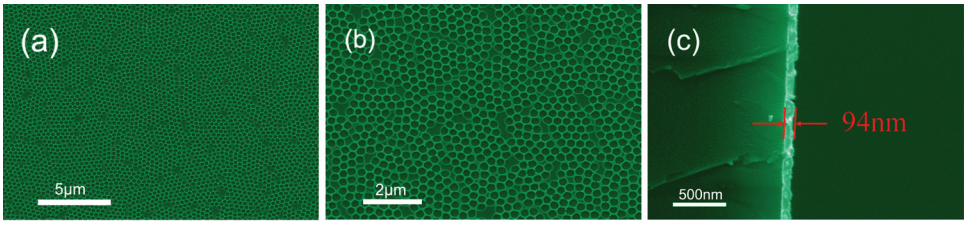

Figure 3. a,b) Surface SEM images of 2D ordered SnO_2 nanofilms and c) cross-sectional SEM image.

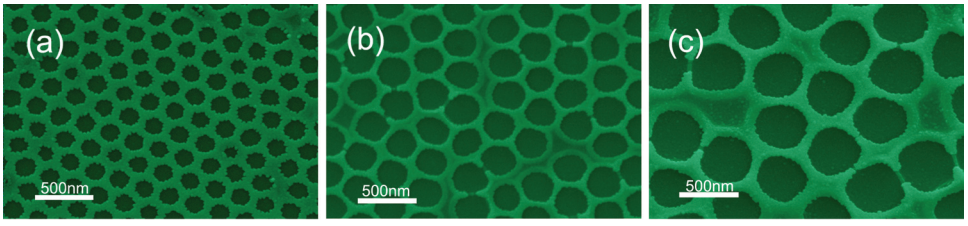

Figure 4. The SEM images of 2D ordered SnO_2 monolayer nanofilms obtained using various sizes of polymer spheres: a) polymer spheres size: 228 nm, hole size: 163 nm; b) polymer spheres size: 308 nm, hole size: 251 nm; and c) polymer spheres size: 490 nm, hole size: 447 nm.

discontinuous network structures, and concentrations above a certain level lead to shrinkage of the hole-wall (Figure S1, Supporting Information). The hole size of 2D ordered SnO_2 nanofilms can be adjusted easily by the mean diameter of the polymer colloidal spheres in monolayer polymer films, as shown in **Figure 4**.

This method can also be extended for fabrication of other 2D ordered semiconducting monolayer nanofilms. When the solutions of TiO_2, ZnO, and CeO_2 precursors were filled into the voids between polymer spheres of monolayer film, corresponding 2D ordered TiO_2, ZnO, and CeO_2 monolayer nanofilms were also fabricated, as shown in **Figure 5**. Their X-ray diffraction (XRD) peaks, shown in **Figure 6**a,b,c, and d can be divided into cassiterite SnO_2 phase (JCPDS 41-1445), rutile/anatase TiO_2 phase (JCPDS 65-0192/JCPDS 21-1272), zincite ZnO phase (JCPDS 36-1451), and CeO_2 phase (JCPDS 65-2975), respectively. Strong and sharp diffraction peaks of the patterns suggest that the as-synthesized metal-oxides are highly crystallized.

2.3. Photoresponse Properties of SnO_2 Nanonets

Furthermore, we took SnO_2 as an example and constructed a photoresponse nanodevice based on 2D ordered SnO_2 monolayer nanofilm, as illustrated in Scheme 1g, since SnO_2 is a very important n-type semiconductor with a large bandgap (i.e., energy gap (E_g) = 3.6 eV at 300 K)[40] and has potential applications in transparent conducting electrodes for organic light-emitting diodes, photodetectors, and solar cells.[41–44]

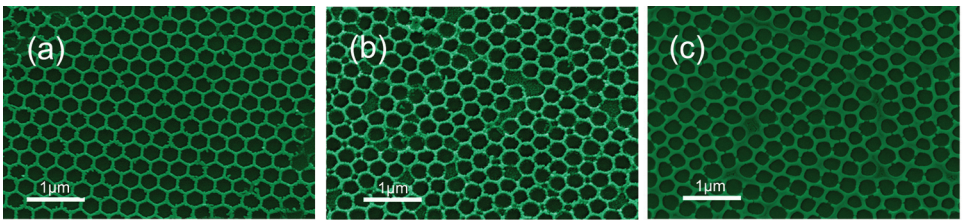

Figure 5. SEM images of other 2D ordered monolayer nanofilms: a) TiO_2, b) ZnO, and c) CeO_2.

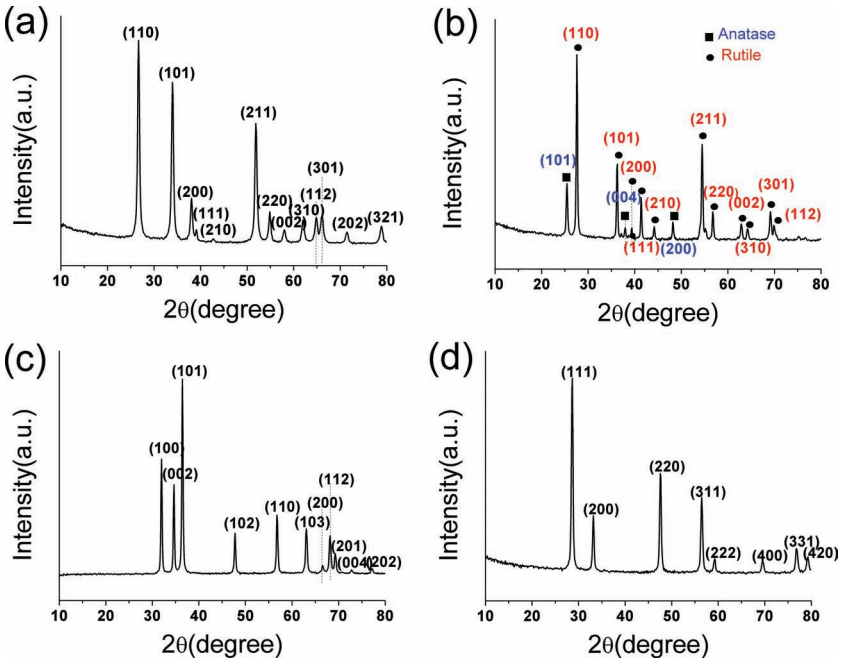

Figure 6. XRD patterns of the as-obtained semiconducting nanfilms: a) SnO_2, b) TiO_2, c) ZnO, and d) CeO_2.

The as-transformed ordered SnO_2 monolayer nanofilm was transported to an electric gun deposition system. The Cr/Au (10/100 nm) electrodes were deposited using 30 μm Au wires as a mask. **Figure 7**a shows a typical SEM image of the photoresponse nanodevice in which the 2D ordered SnO_2 monolayer nanofilm was connected by a pair of electrodes placed 30 μm apart. Figure 7b shows the current–voltage (*I–V*) curves of the photoresponse nanodevice under different light and dark conditions. As shown, the photocurrent increases gradually as light wavelength is reduced from 600 to 320 nm. A photocurrent of as high as 232.3 μA was recorded at a low applied voltage of 1.0 V when illuminated with a 320 nm wavelength light at a density of 0.91 mW cm^{-2}. The photocurrent under 320 nm light irradiation was more than 3.5 times that under dark conditions. The obvious increase in photocurrent under these conditions can be understood by the enhanced number of excited electron–hole pairs when the incident light energy is larger than the bandgap of SnO_2. This can be further confirmed by the spectral photoresponse of the device at a bias of 5.0 V at wavelengths from 210 to 630 nm (**Figure 8**e). At these wavelengths, the photoresponse exhibits a significant increase above the threshold excitation energy of ≈3.6 eV (350 nm), close to the bandgap energy of SnO_2. The responsiveness of the device increases by about three orders of magnitude from as wavelength decreases from 630 to 210 nm.

Moreover, it is known that the work functions of SnO_2 and Cr are ≈4.7 and ≈4.5 eV respectively.[45,46] The linear characteristic of the *I–V* curve is often observed between SnO_2 nanostructures and Cr electrode due to the ohmic contact.[42] However, the *I–V* curve of the present device is nonlinear and asymmetrical. This non-ohmic contact might be attributable to the influence of the surface state (including surface defects, vacancies, and adsorption) of our polycrystalline SnO_2 porous nanofilm. The asymmetry in the *I–V* curves might be due to a difference in roughness between the two nanofilm/metal electrode contact interfaces.[47] It should be noted that the present photocurrent value is about ten times as large as those of other SnO_2 photodetectors (at 1.0 V, with 320 nm light illumination). It is also higher than those of oxide semiconductor photodetectors with different 2D nanostructures, as summarized in **Table 1**. The difference between the dark-current and the photocurrent can reach 166.8 μA. This photoresponse device therefore shows promise as a highly sensitive UV light detector. The as-observed ultrahigh photocurrent may be ascribed to the fact that the photocurrent of the present device is collected from a polycrystallinity SnO_2 nanofilm with continuous network structure rather than an individual nanostructure.

Due to the smooth surface of the as-fabricated SnO_2 nanofilm, a pair of Cr/Au microelectrodes was successfully fabricated on the surface of nanofilm. The distance between the two electrodes decreased from 30 to 1.5 μm. Cr/Au (10/100 nm) microelectrodes were patterned on the top of the SnO_2 monolayer nanofilm using photolithography, electron-beam deposition, and a lift-off process. Representative SEM images of the device at low and high magnification are shown in Figure 8a,b. As expected, both photocurrent and dark current of the device have further

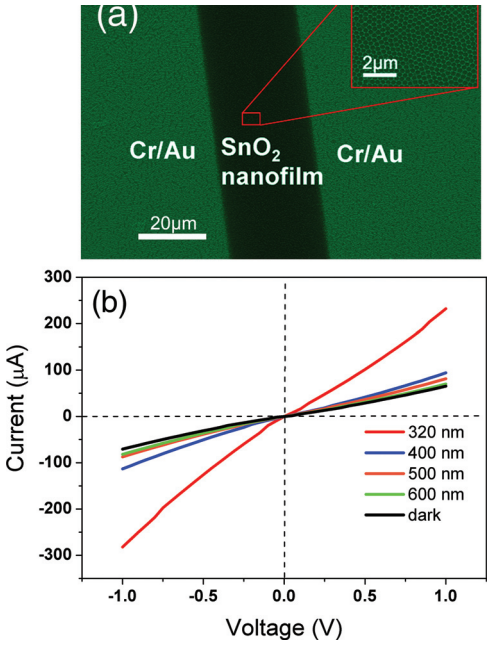

Figure 7. a) Typical SEM image of the 2D ordered SnO_2 monolayer nanofilm-based photoresponse device with electrodes distance ≈ 30 μm. b) The *I–V* characteristics of the devices illuminated with different wavelength lights and under dark condition.

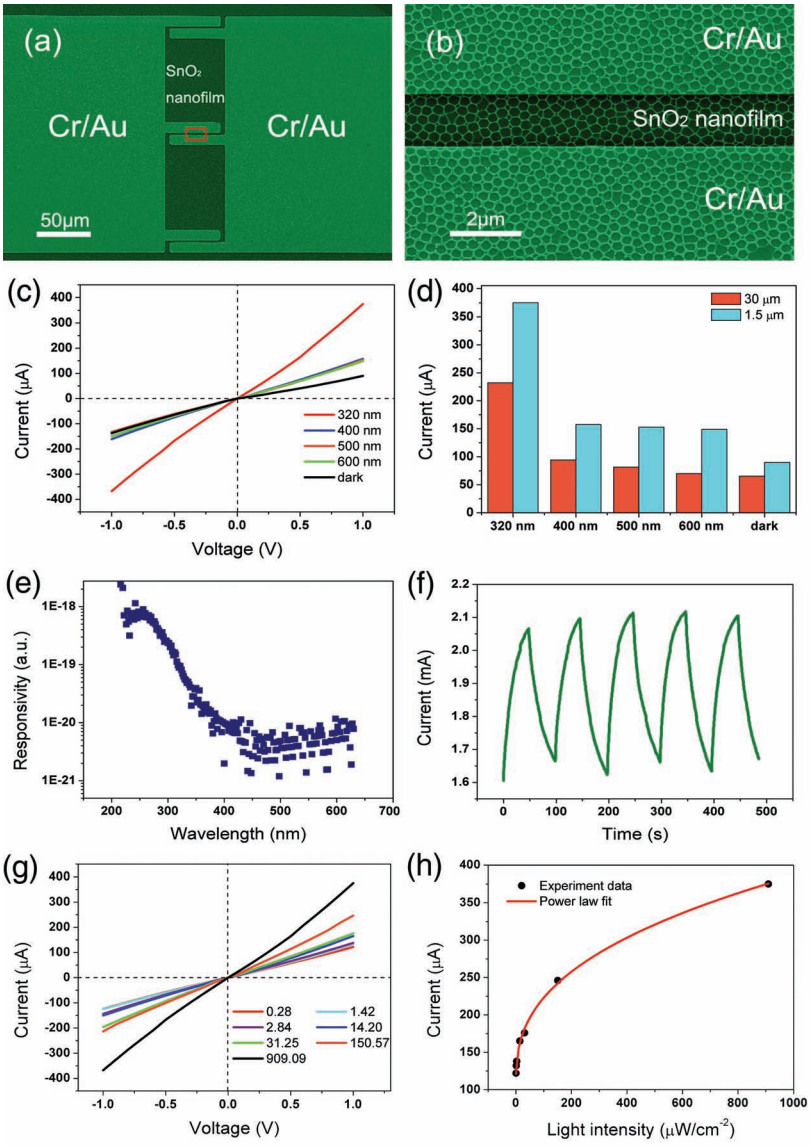

Figure 8. a) Typical SEM image of the 2D ordered SnO_2 monolayer nanofilm-based photoresponse device with electrodes distance ≈1.5 μm. b) An amplified image of photoresponse device (red box in (a)). c) The *I–V* characteristics of the devices illuminated with different wavelength lights and under dark condition. d) The comparison of photocurrent of two photoresponse devices measured at a bias of 1.0 V with different wavelength lights and under dark condition. e) Spectral photoresponse of the device measured at a bias of 5.0 V at diffraction wavelengths ranging from 210 to 630 nm. f) Time-dependent response of the photoresponse device measured under air conditions at a bias of 5.0 V, the light power intensity was kept at 0.91 mW cm^{-2} when the UV light was turned on. g) *I–V* characteristics of the device under 320 nm light irradiation with various power intensities. h) The light-intensity-dependent photocurrent of the device at an excitation wavelength of 320 nm and bias of 1.0 V, the solid line shows a fitting of power function law $C = 109.78\ 19.00 \times P^{0.39}$, from the experimental data. All data were obtained at photoresponse device with electrodes distance ≈1.5 μm.

increase (lower resistance) by comparing with the device with electrodes distance of 30 μm, as shown in Figure 8c,d. However, the increases in photocurrent at different wavelengths were found to be greater than under dark current conditions. The photocurrent under 320 nm light irradiation was 4.1 times that under dark current conditions. The difference between the dark-current and the photocurrent reached 285.3 μA, as shown in Figure 8c and Table 1. Obviously, the photoresponse sensitivity of the device can be further enhanced by decreasing the distance between the electrodes. This improved sensitivity might be attributable to increased photoelectric conversion efficiency caused by a SnO_2 network with fewer structural defects, allowing the electrodes to be placed closer together. The *I–V* curves of the photoresponse device based on monolayer SnO_2 nanonets with poor network structure were also measured (Figure S2, Supporting Information). Compared with the photoresponse device with good SnO_2 network structure, both photocurrent (at 1.0 V, with 320 nm light illumination) and dark-current of device decreased about nine times. This further displays that the improvement of structural regularity of semiconductor materials is an important path to fabricate high-performance photodetector.

The time-dependent photoresponse of the device is shown in Figure 8f. This was measured by periodically the 320 nm light on and off under air conditions. Upon illumination, the photocurrent increased to a stable value of 2.1 mA and then decreased dramatically to its initial value when the light was turned off. This showed its excellent stability and reproducibility.

To determine the ability of the device to respond to the intensity of the light, we irradiated it with 320 nm light at power intensities ranging from 0.28 to 909.09 μW cm^{-2}. The resulting *I–V* curves are shown in Figure 8g. The results demonstrated that the photocurrent of the as-fabricated device was quite dependent on light intensity. The fitting of the dependence of photocurrent to the light intensity gave a power function law, $C \propto P^{0.39}$, where *C* is the photocurrent value and *P* is the light intensity (Figure 8h). The non-unity exponent was a result of the complex process of electron–hole generation, trapping, and recombination within the semiconductor.[48] By adjusting the intensity of illumination, the current can be reversibly changed 2 to 3 times without damaging the nanofilm. This photoresponse device can be said to be very promising as a quantitative UV light detector.

3. Conclusion

This study shows that 2D ordered porous SnO_2 monolayer nanofilms and even other 2D ordered porous semiconducting metal-oxide nanofilms such as TiO_2, ZnO, and CeO_2 can be

Table 1. Comparison of the characteristic parameters for inorganic semiconductor nano-photodetectors obtained in the present work and previous reports.[a)]

Photodetectors	Dark current (at 1.0 V)	Photocurrent (at 1.0 V)	Ref.
SnO_2 nanowire	40.0 nA (at 0.1 V)	200.0 nA (at 0.1 V)	[49]
SnO_2 nanowire	19.4 nA	2.1 μA	[42]
SnO_2 nanowire array	77.0 μA (at 12.0 V)	130.0 μA (at 12.0 V)	[50]
Sb-doped SnO_2 nanowire	2.0 pA	1.0 μA	[51]
V_2O_5 nanowire	12.5 nA	25.8 nA	[52]
SnO_2 nanobelt	0.4 nA (at –5.0 V)	80.0 μA (at –5.0 V)	[53]
CdS nanobelt	5.0 μA	30.0 μA	[54]
$In_2Ge_2O_7$ nanobelt	–	19.0 nA (at 5.0 V)	[55]
$NiCo_2O_4$ platelets nanofilm	0.6 μ A	1.4 μ A	[38]
ZnO hollow-sphere nanofilm	50.0 nA (at 5.0 V)	2.6 μ A (at 5.0 V)	[39]
SnO_2 monolayer nanofilm (electrodes distance ≈ 30 μm)	65.5 μA	232.3 μA	Present work
SnO_2 monolayer nanofilm (electrodes distance ≈ 1.5 μm)	89.9 μA	375.2 μA	Present work

[a)]The dark and photocurrent were measured at 1.0 V unless specifically noted.

fabricated easily using polymer monolayer nanofilms prepared from oil–water interfacial self-assembly as sacrificial templates. The pore sizes of the nanonets can be adjusted by the diameters of polymer particles in the template. We constructed a SnO_2 nanonet-based UV photodetector and found it to exhibit ultrahigh photocurrent and sensitivity, excellent stability, and reproducible characteristics. It may have applications in high-performance photodetectors, photoelectronic switches, and solar cells.

4. Experimental Section

Materials: Styrene (CP), acrylic acid (CP), tin tetrachloride [$SnCl_4{\cdot}5H_2O$], cerium nitrate [$Ce(NO_3)_3{\cdot}6H_2O$], zinc acetate [$Zn(CH_3COO)_2{\cdot}2H_2O$], titanium butoxide, acetylacetone, citric acid monohydrate, ammonium persulfate (APS), absolute ethanol, and hexane were purchased from Sinopharm Chemical Reagent Corp. and used as received.

Synthesis of Colloidal Polymer Sphere: Monodispersed poly(styrene-*co*-acrylic acid) (PSA) spheres with a diameter of approximately 308 nm, as determined by SEM, were synthesized by emulsion polymerization of styrene and acrylic acid. Briefly, styrene (5 g), acrylic acid (0.5 g), and deionized water (80 g) were charged into a round-bottom flask (250 mL) equipped with a mechanical stirrer, thermometer with a temperature controller, N_2 inlet, Graham condenser, and heating mantle. This mixture was stirred (≈180 rpm) and deoxygenated by bubbling nitrogen gas at room temperature for 0.5 h. It was then heated to 75 °C, followed by addition of aqueous APS solution (0.100 g of APS in 5 g of water). This reaction was conducted at 75 °C for another 0.5 h under a slow stream of N_2. Then styrene (15 g) was slowly, continuously added to the system over a period of 2 h. After that, the flask was kept at 75 °C for 5 h before being allowed to cool to room temperature under a nitrogen purge. The resultant colloidal suspensions of PSA spheres were filtered to remove any large agglomerates. They were then stored in polyethylene terephthalate (PET) plastic bottles for later use (solid content: 10.4%). PSA colloids of other sizes could be obtained by adjusting the ratio of styrene to acrylic acid.

Fabrication of Polymer Monolayer Nanofilm: Polymer monolayer nanofilm was fabricated using the oil–water interfacial self-assembly method. In a typical experiment, polymer colloid (0.05 mL) was dispersed in deionized water (40 mL, concentration: 0.013%), followed by the addition of hexane (10 mL) to produce a hexane/water interface. When ethanol (2.0 mL) was added to the interface at a low rate (4.0 mL h^{-1}), the polymer colloidal spheres were immediately trapped at the interface. After most of the hexane at the top of the vessel was carefully removed by syringe, the densely packed monolayer nanofilm was transferred to a Si/SiO_2 substrate (a thermally oxidized Si substrate covered with a 200 nm SiO_2 layer) and then dried at room temperature to produce a monolayer nanofilm.

Fabrication of Monolayer SnO_2 Nanonet: A 2D ordered SnO_2 monolayer nanofilm was prepared by filling the voids of polymer nanofilm with a tin oxide sol-gel precursor, then calcining the resulting composite at 600 °C to remove polymer template. Briefly, the polymer monolayer nanofilm from a Si/SiO_2 substrate was partially vertically dipped into a tin oxide sol-gel precursor solution containing $SnCl_4{\cdot}5H_2O$ (2.104 g) and citric acid monohydrate (1.261 g) in absolute ethanol (100 mL) for 30 s, and then left for hydrolysis and condensation in air at 40 °C for 10 h. The resultant SnO_2/polymer composite was then calcined in air from 40 to 600 °C at 1°C min^{-1} and kept at 600 °C for 3 h. It was finally allowed to cool to room temperature. The as-obtained 2D ordered SnO_2 monolayer nanofilm was semitransparent under incident white light. When tin oxide sol-gel precursor solution was replaced by titanium oxide precursor solution (1.702 g titanium butoxide, 2.002 g acetylacetone, and 100 mL absolute ethanol), zinc oxide precursor solution (1.098 g $Zn(CH_3COO)_2{\cdot}2H_2O$ and 100 mL absolute ethanol), and ceria precursor solution (2.171 g $Ce(NO_3)_3{\cdot}6H_2O$, 1.051 g citric acid monohydrate, and 100 mL absolute ethanol), 2D ordered TiO_2, ZnO and CeO_2 monolayer nanofilms could also be fabricated using this method.

Construction of Monolayer SnO_2 Nanonet-Based Nanodevice: The as-transformed ordered SnO_2 monolayer nanofilm was transported to an electric gun deposition system (ULVAC UEP-3000-2C). The Cr/Au (10/100 nm) electrodes (distance ≈ 30 μm) were deposited using 30 μm Au wires as a mask. The Cr/Au (10/100 nm) microelectrodes (distance ≈1.5 μm) were patterned on the top of the SnO_2 monolayer nanofilms using optical lithography with the assistance of a pre-designed mask and electron-beam deposition followed by a lift-off process. The *I–V* characteristics of SnO_2 monolayer nanofilm were measured using an Advantest picoammeter R8340A and a dc voltage source R6144. A spectral response for different wavelengths was recorded by using a xenon lamp (500 W).

The time-dependent photoresponses of the device were measured using a current meter after shutting off the UV light. The incident light power was calibrated using an UV enhanced Si photodiode.

Characterization: SEM was conducted with a Philips XL 30 field emission microscope at an accelerating voltage of 10 kV. The phase of the samples was determined using a Rigaku D/max-rB X-ray diffractometer using Cu Kα radiation (λ = 1.5406 Å). Because the obtained signals of as-prepared monolayer nanonets are very weak and can be affected by Si/SiO_2 substrate signals, the X-ray diffraction (XRD) measurements of porous metal-oxide semiconductor powders from multilayer metal-oxide nanonets were carried out. Multilayer metal-oxide nanonets were fabricated by filling the voids of multilayer polymer colloid nanofilms (preparation by repeated deposition of monolayer polymer colloid film) with oxide precursor solutions, followed by calcination in air.

Supporting Information

Supporting Information is available from the Wiley Online Library or from the author.

Acknowledgements

Financial supports of this research from the National Natural Science Foundation of China (Grant Nos. 51133001, 91123006, 21001028, 51002032 and 21074023), Shanghai Science and Technology Foundation (10JC1401900), Science and Technology Foundation of Ministry of Education of China (IRT0911, 20110071130002), and Shanghai Chenguang Foundation (11CG06) are appreciated.

Received: October 18, 2011
Revised: December 3, 2011
Published online: January 23, 2012

[1] R. Gordon, D. Sinton, K. L. Kavanagh, A. G. Brolo, *Acc. Chem. Res.* **2008**, *41*, 1049.
[2] T. W. Ebbesen, H. J. Lezec, H. F. Ghaemi, T. Thio, P. A. Wolff, *Nature* **1998**, *391*, 667.
[3] Q. Liao, Y. Wang, J. Li, K. Wu, X. C. Ai, J. P. Zhang, *Appl. Phys. Lett.* **2007**, *91*, 041103.
[4] L. Pang, G. M. Hwang, B. Slutsky, Y. Fainman, *Appl. Phys. Lett.* **2007**, *91*, 123112.
[5] L. Pang, K. A. Tetz, Y. Fainman, *Appl. Phys. Lett.* **2007**, *90*, 111103.
[6] J. M. Park, S. G. Lee, H. R. Park, M. H. Lee, *J. Opt. Soc. Am. B* **2010**, *27*, 2247.
[7] A. G. Brolo, E. Arctander, R. Gordon, B. Leathem, K. L. Kavanagh, *Nano Lett.* **2004**, *4*, 2015.
[8] G. Hong, C. Li, Q. Limin, *Adv. Funct. Mater.* **2010**, *20*, 3774.
[9] E. Chow, A. Grot, L. W. Mirkarimi, M. Sigalas, G. Girolami, *Opt. Lett.* **2004**, *29*, 1093.
[10] A. Lesuffleur, H. Im, N. C. Lindquist, S. H. Oh, *Appl. Phys. Lett.* **2007**, *90*, 243110.
[11] J. Henzie, M. H. Lee, T. W. Odom, *Nat. Nanotechnol.* **2007**, *2*, 549.
[12] Y. C. Liao, C. H. Lin, S. L. Wang, *J. Am. Chem. Soc.* **2005**, *127*, 9986.
[13] S. Kuiper, C. J. M. vanRijn, W. Nijdam, M. C. Elwenspoek, *J. Membrane. Sci.* **1998**, *150*, 1.
[14] A. M. Prenen, J. C. A. H. van der Werf, C. W. M. Bastiaansen, D. J. Broer, *Adv. Mater.* **2009**, *21*, 1751.
[15] J. Henzie, J. E. Barton, C. L. Stender, T. W. Odom, *Acc. Chem. Res.* **2006**, *39*, 249.
[16] T. Wang, X. Li, J. Zhang, Z. Ren, X. Zhang, X. Zhang, D. Zhu, Z. Wang, F. Han, X. Wang, B. Yang, *J. Mater. Chem.* **2010**, *20*, 152.
[17] F. Sun, W. Cai, Y. Li, B. Cao, Y. Lei, L. Zhang, *Adv. Funct. Mater.* **2004**, *14*, 283.
[18] Y. H. Cho, G. Cho, J. S. Lee, *Adv. Mater.* **2004**, *16*, 1814.
[19] J. M. McLellan, M. Geissler, Y. Xia, *J. Am. Chem. Soc.* **2004**, *126*, 10830.
[20] P. Jiang, *Angew. Chem. Int. Ed.* **2004**, *43*, 5625.
[21] T. Ding, K. Song, K. Clays, C.-H. Tung, *Adv. Mater.* **2009**, *21*, 1936.
[22] T. Ding, F. Wang, K. Song, G. Yang, C.-H. Tung, *J. Am. Chem. Soc.* **2010**, *132*, 17340.
[23] S. Zhang, L. Chen, S. Zhou, D. Zhao, L. Wu, *Chem. Mater.* **2010**, *22*, 3433.
[24] Z. Niu, J. He, T. P. Russell, Q. Wang, *Angew. Chem. Int. Ed.* **2010**, *49*, 10052.
[25] C. N. R. Rao, K. P. Kalyanikutty, *Accounts. Chem. Res.* **2008**, *41*, 489.
[26] L. Hu, M. Chen, X. Fang, L. Wu, *Chem. Soc. Rev.* DOI:10.1039/C1CS15189D.
[27] H. Duan, D. Wang, D. G. Kurth, H. Möhwald, *Angew. Chem. Int. Ed.* **2004**, *43*, 5639.
[28] F. Reincke, S. G. Hickey, W. K. Kegel, D. Vanmaekelbergh, *Angew. Chem. Int. Ed.* **2004**, *43*, 458.
[29] Y. J. Li, W. J. Huang, S. G. Sun, *Angew. Chem. Int. Ed.* **2006**, *45*, 2537.
[30] P. Arumugam, D. Patra, B. Samanta, S. S. Agasti, C. Subramani, V. M. Rotello, *J. Am. Chem. Soc.* **2008**, *130*, 10046.
[31] L. Xu, G. Han, J. Hu, Y. He, J. Pan, Y. Li, J. Xiang, *Phys. Chem. Chem. Phys.* **2009**, *11*, 6490.
[32] J. Wang, D. Wang, N. S. Sobal, M. Giersig, M. Jiang, H. Möhwald, *Angew. Chem. Int. Ed.* **2006**, *45*, 7963.
[33] L. M. Goldenberg, J. Wagner, J. Stumpe, B. R. Paulke, E. Gornitz, *Langmuir* **2002**, *18*, 5627.
[34] C. Zhang, X. Zhang, X. Zhang, X. Ou, W. Zhang, J. Jie, J. C. Chang, C. S. Lee, S. T. Lee, *Adv. Mater.* **2009**, *21*, 4172.
[35] S. Biswas, L. T. Drzal, *Nano Lett.* **2008**, *9*, 167.
[36] L. Hu, R. Ma, T. C. Ozawa, F. Geng, N. Iyi, T. Sasaki, *Chem. Commun.* **2008**, 4897.
[37] L. Hu, R. Ma, T. C. Ozawa, T. Sasaki, *Angew. Chem. Int. Ed.* **2009**, *48*, 3846.
[38] L. Hu, L. Wu, M. Liao, X. Fang, *Adv. Mater.* **2011**, *23*, 1988.
[39] M. Chen, L. Hu, J. Xu, M. Liao, L. Wu, X. Fang, *Small* **2011**, *7*, 2449.
[40] T. Zhai, X. Fang, M. Liao, X. Xu, H. Zeng, B. Yoshio, D. Golberg, *Sensors* **2009**, *9*, 6504.
[41] D. Vaufrey, M. Ben Khalifa, M. P. Besland, C. Sandu, M. G. Blanchin, V. Teodorescu, J. A. Roger, J. Tardy, *Synth. Met.* **2002**, *127*, 207.
[42] L. Hu, J. Yan, M. Liao, L. Wu, X. Fang, *Small* **2011**, *7*, 1012.
[43] S. Chappel, S. G. Chen, A. Zaban, *Langmuir* **2002**, *18*, 3336.
[44] F. Yang, S. R. Forrest, *Adv. Mater.* **2006**, *18*, 2018.
[45] M. Batzill, U. Diebold, *Prog. Surf. Sci.* **2005**, *79*, 47.
[46] H. L. Skriver, N. M. Rosengaard, *Phys. Rev. B* **1992**, *46*, 7157.
[47] H. C. Liu, Z. R. Wasilewski, M. Buchanan, H. Chu, *Appl. Phys. Lett.* **1993**, *63*, 761.
[48] H. Kind, H. Yan, B. Messer, M. Law, P. Yang, *Adv. Mater.* **2002**, *14*, 158.
[49] C. H. Lin, R. S. Chen, T. T. Chen, H. Y. Chen, Y. F. Chen, K. H. Chen, L. C. Chen, *Appl. Phys. Lett.* **2008**, *93*, 112115.
[50] J. M. Wu, C. H. Kuo, *Thin Solid Films* **2009**, *517*, 3870.
[51] Q. Wan, E. Dattoli, W. Lu, *Small* **2008**, *4*, 451.
[52] T. Zhai, H. Liu, H. Li, X. Fang, M. Liao, L. Li, H. Zhou, Y. Koide, Y. Bando, D. Golberg, *Adv. Mater.* **2010**, *22*, 2547.
[53] Y. J. Chen, C. L. Zhu, M. S. Cao, T. H. Wang, *Nanotechnology* **2007**, *18*, 285502
[54] L. Li, P. Wu, X. Fang, T. Zhai, L. Dai, M. Liao, Y. Koide, H. Wang, Y. Bando, D. Golberg, *Adv. Mater.* **2010**, *22*, 3161.
[55] L. Li, P. S. Lee, C. Yan, T. Zhai, X. Fang, M. Liao, Y. Koide, Y. Bando, D. Golberg, *Adv. Mater.* **2010**, *22*, 5145.